Lab on a Chip

CrossMark
click for updates

Assembly of multiple cell gradients directed by three-dimensional microfluidic channels†

Yiwei Li,‡ Xiaojun Feng,‡ Yachao Wang, Wei Du, Peng Chen, Chao Liu and Bi-Feng Liu*

Active control over the cell gradient is essential for understanding biological systems and the reconstitution of the functionality of many types of tissues, particularly for organ-on-a-chip. Here, we propose a three-dimensional (3D) microfluidic strategy for generating controllable cell gradients. In this approach, a homogeneous cell suspension is loaded into a 3D stair-shaped PDMS microchannel to generate a cell gradient within 10 min by sedimentation. We demonstrate that cell gradients of various profiles (exponential and piecewise linear) can be achieved by precisely controlling the height of each layer during the fabrication. With sequential seeding, we further demonstrate the generation of two overlapping cell gradients on the same glass substrate with pre-defined designs. The cell gradient-based QD cytotoxicity assay also demonstrated that cell behaviors and resistances were regulated by the changes in cell density. These results reveal that the proposed 3D microfluidic strategy provides a simple and versatile means for establishing controllable gradients in cell density, opening up a new avenue for reconstructing functional tissues.

Introduction

Cell gradients are often found in tissues such as the interface between various layers of the skin and the junction of non-mineralized and mineralized tissues in the tendon-to-bone insertion and liver sinusoid in whole liver.[1–5] These gradients in cell density lead to the establishment of gradations in biochemical or extracellular matrix (ECM) cues, resulting in regulation of cell–cell interactions and variations in cell functions, such as migration, proliferation and differentiation.[6–8] Active control over the cell gradient may provide a valuable means for understanding the functions of biological systems and for the recreation of the functionality of many types of tissues.[9,10]

To date, a variety of methods have been proposed to establish controllable gradients in cell density, exploiting the differential migration of cells on a surface in the presence of mechanical, chemical and electrical cues.[11–15] However, these methods suffer from issues such as prolonged cell migration time, low controllability and reproducibility. The reason might be the intrinsic properties of the cell migration behavior.[16] Alternatively, Xia's group developed a simple and

versatile approach for generating cell gradients in two hours by tilting a glass substrate into a homogeneous cell suspension.[17] Yang *et al.* lately explored the use of the topographic effect of the gradient nanodendrites to establish controllable gradients in cell density within half an hour.[18] These methods represent a significant advance in establishing cell gradients. However, it remains a great challenge to achieve multiple overlapping cell gradients of pre-defined designs.

Advances in microfluidic systems and microscale technologies provide new opportunities for reconstructing functional tissues *in vitro*.[19–21] For example, "organ-on-a-chip", a biomimetic microsystem integrated with tissue structures and functions, impacts a variety of fields, including toxicology, pharmaceuticals and cosmetics.[22] A variety of organ functions have been reconstituted, including heart,[23] lung,[24] marrow[25] and liver,[26,27] in which tissue–tissue interfaces play a critical role.[24] Cell gradients of a single-cell type have been established in microfluidic chips for various applications such as investigation of nanocytotoxity.[28–30] However, it is still a great challenge to develop an interface tissue structure with overlapping cell gradients for reconstitution of interface tissue structures. Here, we demonstrate a 3D microfluidic strategy for assembling controllable gradients in cell density with user-defined designs.

As shown in Fig. 2a, a 3D stair-shaped PDMS microchannel is reversibly bonded to a glass substrate to form the microfluidic device. After loading of homogeneous cell suspension into the microchannel, cells will shortly settle on the glass substrate by gravity and a gradient in cell density can

Britton Chance Center for Biomedical Photonics at Wuhan National Laboratory for Optoelectronics – Hubei Bioinformatics & Molecular Imaging Key Laboratory, Systems Biology Theme, Department of Biomedical Engineering, College of Life Science and Technology, Huazhong University of Science and Technology, Wuhan 430074, China. E-mail: bfliu@mail.hust.edu.cn

‡ These authors contributed equally to this work.

be established due to the increasing volumes of cell suspensions along the stair. Theoretically, the cell density at the nth step is equal to the density of the cell suspension multiplied by the height of the nth step (the vertical distance from the substrate to the ceiling of the microchannel at the nth step). Thus, by simply varying the step heights and the design of the microchannel, cell gradients of user-defined designs can be further achieved. A cell gradient-based assay was further carried out. The results demonstrated that cell behaviors were regulated by the changes in cell density. The QD cytotoxicity assay also demonstrated the cell density-dependent results. Conclusively, the proposed 3D microfluidic strategy offers a simple and versatile means for controllable generation of gradients in cell density, providing a new avenue for reconstructing functional tissues.

Materials and methods

Materials and reagents

Chemicals including Na_2HPO_4, KH_2PO_4, NaOH, NaCl, $CaCl_2$, KCl, HCl, $MgCl_2$, and D-glucose were purchased from Sinopharm Chemical Reagent (Shanghai, China). Reagents such as poly-L-lysine (MW, 150 000–300 000), fibronectin, penicillin, streptomycin, trimethyl chlorosilane, 4-(2-hydroxyethyl)-1-piperazineethanesulfonic acid (HEPES), and dimethyl sulfoxide (DMSO) were purchased from Sigma-Aldrich (St. Louis, MO). DNA fluorescent dye propidium iodide was obtained from Beijing Biosynthesis Biotechnology Co., Ltd. (Beijing, China). Cell membrane dyes DiO (1,1′-dioctadecyl-3,3,3′,3′-tetramethylindocarbocyanine perchlorate) and DiI (3,3′-dioctadecyloxacarbocyanine perchlorate) were purchased from Beyotime Institution of Biotechnology Co., Ltd. (Beijing, China). Calcein-AM and Fluo-3/AM were obtained from Biotium (Hayward, CA). Phosphate-buffered saline (PBS) solution contained 135 mM NaCl, 2.7 mM KCl, 1.5 mM KH_2PO_4, and 8 mM K_2HPO_4 (pH 7.2). Poly-L-lysine (MW, 150 000–300 000) was prepared in PBS solution with a final concentration of 0.1% (w/v). Fibronectin was prepared in PBS solution with a final concentration of 20 $\mu g\ mL^{-1}$. Stock solutions of fluorescent dyes, including propidium iodide, Fluo-3/AM, DiO and DiI, were prepared in DMSO. Fluorescent dyes were diluted in PBS solution from the stock solution prior to use. All solutions were prepared with water purified by the Direct-Q system (Millipore, Bedford, MA, USA) and filtered with 0.45 μm syringe filters prior to use.

Chip design and soft lithography fabrication

Three-dimensional (3D) microfluidic chips were fabricated with poly(dimethylsiloxane) (PDMS) as the structural materials using soft lithography and rapid prototyping method (Fig. S1†). In brief, an SU-8 (GM1070, Gersteltec Sarl, Switzerland) mold was fabricated on a 3-inch silicon wafer layer by layer through multilayer soft lithography. A PDMS microchannel was formed by prototyping the SU-8 mold. Through diaphragm holes were punched at each end of the microchannels as the world-to-chip interface. The PDMS layer was then reversibly bonded to a glass substrate to form the final device.

Paper-based fabrication

A paper-based prototyping method was developed to fabricate 3D PDMS microchannels with large heights (Fig. 1), such as the microchannels used in Fig. 3 and 5. To fabricate 3D microchannels, a commercial A4 paper (70 g m^{-2}) was cut into small pieces according to the designs of each layer of the microchannel. Layers of paper sheets were assembled together by glue to form the paper mold on a silicon substrate. The paper mold was pretreated with trimethyl chlorosilane prior to use. PDMS was poured onto the paper mold and cured at 65 °C for 3 hours to form the 3D microchannel. The PDMS layer was peeled off from the mold, and through diaphragm holes were punched at each end of the microchannels as the world-to-chip interface. The PDMS layer was then reversibly bonded to a glass substrate to form the final device.

3D printing-based mold fabrication

A microfluidic mold with a smooth profile was fabricated using the 3D printing method. 3D printing was performed on the experimental 3D printer (Makerbot Replicator 2X) using a 1.75 mm (acrylonitrile–butadiene–styrene copolymer) filament (MakerBot). ABS slurry (20% w/v ABS in acetone) was used in place of the support material while printing. The 3D printer used in this work has a positioning precision of 11 μm in the XY-axis and 2.5 μm in the Z-axis. The layer resolution is 100 μm.

Optical imaging system

An inverted fluorescence microscope (IX71, Olympus, Japan) with a CCD camera (Evolve 512, Photometrics, USA) was used for imaging. Cell distributions were observed under a 10× objective lens (N.A. 0.3) with a filter cube of U-MWIB2 (460–490 nm band-pass filter, 505 nm diachronic mirror, 510 nm high-pass filter, Olympus, Japan) for Fluo-3-labeled NIH 3T3 and DiO-labeled HepG2 and a filter cube of U-MWG2 (510–550 nm band-pass filter, 570 nm diachronic mirror, 590 nm high-pass filter, Olympus, Japan) for DiI-labeled NIH 3T3.

Cell culture and maintenance

NIH 3T3 fibroblasts and HepG2 cells were maintained in Dulbecco's modified Eagle's medium (DMEM, Gibco) supplemented with 10% (v/v) fetal bovine serum (NCS, Gibco), 100 U mL^{-1} penicillin and streptomycin at 37 °C in a humidified atmosphere of 5% CO_2. Cells were subcultured at a ratio of 1 : 3 every 3 days to maintain cells in the exponential growth phase. Cells were harvested by treatment with 0.2% trypsin–EDTA solution (Gibco) and suspended in culture media.

Cell counting method

Harvested cells were counted using a standard hemocytometer technique and further diluted with DMEM to the final
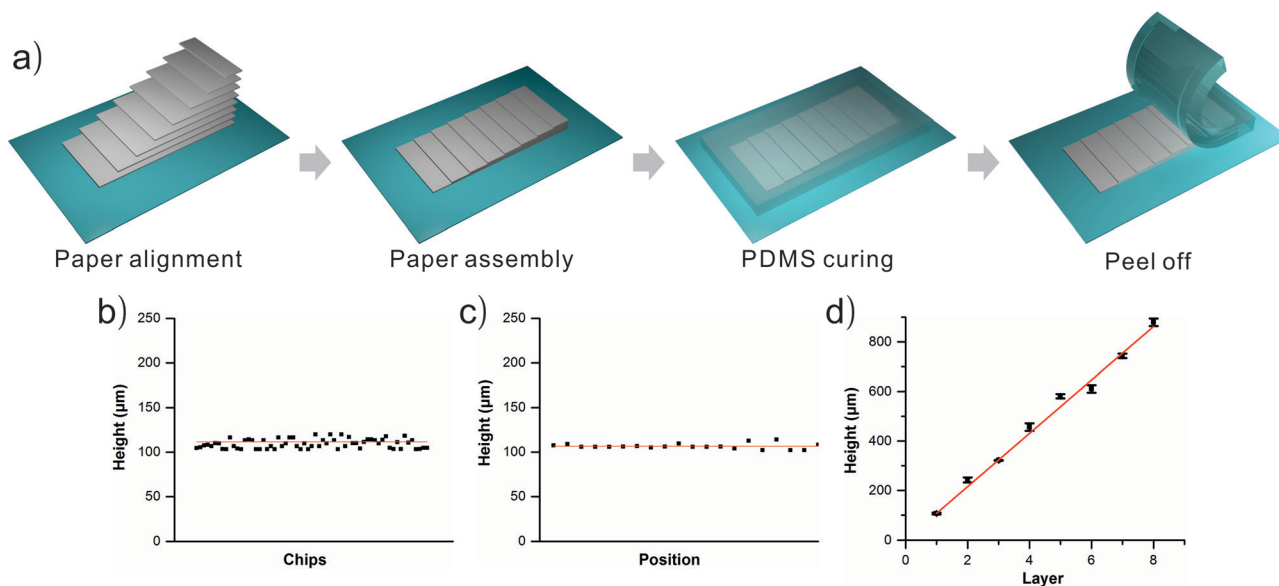
Fig. 1 Fabrication of three-dimensional microfluidic chips. (a) Schematic illustrating the fabrication process using the paper-based prototyping method. (b) The variation in the height of the microchannel among chips. (c) The variation in the height of the microchannel within a chip. (d) The height of each step of a stair-shaped microchannel with a linear profile fabricated using the paper-based prototyping method. The height of each step was measured three times using an optical microscope.

concentrations for experiments. To determine the cell density at each step of the stair-shaped microchannels, cells at 9 random locations of each step were counted, and the cell density was calculated as the mean value of the 9 counts divided by the field of view area.

Cell loading and culture on chip

Before loading of cells, PDMS microchannels were treated with oxygen plasma to enhance the hydrophilic behavior and were sterilized with 75% ethanol for 15 minutes. After removal of ethanol, microchannels were incubated with 0.1% (w/v) poly-L-lysine (MW: 150 000–300 000) and fibronectin (20 μg mL^{-1}) at 37 °C for 2 hours and sequentially rinsed with buffer solutions and cell culture media. Cell suspension was then added to the inlet. Cells were transported into the 3D microchannel by applying a negative pressure of −0.6 kPa on the outlet. After the microchannel was fully filled with the homogeneous cell suspension, the microfluidic device was incubated at 37 °C under a 5% CO_2 atmosphere for 10 min, allowing sedimentation of the cells. Cells were further incubated for 2 more hours for full attachment to the substrate. After removal of the reversibly bonded PDMS layer, a glass substrate with cell gradients was achieved. A sequential seeding process was used for generating overlapping cell gradients of different cell types.

Cell viability assay

Dead/Live assay was carried out to examine the viability of the cells. After the establishment of cell gradients, the microfluidic device was incubated for 10 h at 37 °C under a 5% CO_2 atmosphere. Calcein-AM (20 μM) and PI (2.5 μg mL^{-1}) were then added to stain the cells. After incubation for

another 20 min, cells were gently rinsed with the culture medium to remove residual fluorescent dyes.

Cell proliferation assay

Cell gradient was firstly fixed with 1% paraformaldehyde at room temperature for 1 hour. After rinsing with PBS buffer, the cell gradient was stained with rabbit anti-Ki67 for 2 hours at 37 °C. After rinsing, the cell gradient was incubated with secondary antibody goat anti-rabbit Cy3 for 1 hour at room temperature. DAPI was used as a nuclear counterstain. After rinsing, the cell gradient was visualized under a fluorescence microscope.

Cytotoxicity of the nano-QD assay on the microfluidic chip

CdTe QDs coated with carboxyl groups (noted as CdTe-COOH QDs) was used in this study. Prior to use, a stock solution of CdTe-COOH QDs was diluted into the desired concentrations (0, 10, 20, and 30 μg mL^{-1}) using DMEM cell culture medium. After the cell gradient has been incubated for 6 hours, QD solutions were infused into the channels for 24 hour culturing. Live/Dead assay was carried out to detect cell viability. The results were visualized under an inverted fluorescence microscope.

Results

Fabrication of three-dimensional microfluidic devices

Three-dimensional microfluidic chips were fabricated for assembly of cell gradients. Two different strategies were used here for the fabrication of different shapes. Soft lithography and rapid prototyping were employed to fabricate a three-dimensional chip with a height less than 1000 μm (Fig. S1†).

A stair-shaped chip with a higher height was fabricated using a novel paper-based fabrication method (Fig. 1). Commercial A4 paper (70 g m^{-2}) was cut into paper sheets according to the design of each layer of the microchannel. Layers of paper sheets were assembled by glue to form the paper mold on a silicon substrate. Prior to rapid prototyping, the paper-based mold was preconditioned with trimethyl chlorosilane. PDMS was used to fabricate the final device through the rapid prototyping method.

Next, we studied whether the paper-based prototyping method was suitable for fabricating 3D PDMS microchannels. After fabrication using the paper-based prototyping method, a 3D PDMS microchannel was cut for measurement under an optical microscope. Microchannels with a single layer were firstly fabricated. The heights of the microchannels were measured, and the results are summarized in Fig. 1b and c, which show variations in the microchannel height among chips and within a chip. A stair-shaped microchannel with a linear profile was then fabricated. The height of each step was measured three times, and the results are shown in Fig. 1d. The RSD for the height of each step was less than 3.4%. The heights of the eight steps could be well fitted with a linear function with a correlation coefficient of 0.999. The slope of the linear regression was 107.4, which was in close agreement with the measured paper thickness of 102.0 μm (without accounting for the glue). These results validated that the paper-based prototyping method could be used to fabricate 3D PDMS microchannels for cell gradient establishment.

Finally, a 3D printing method was employed to fabricate the molds for prototyping the microchannels to achieve cell gradients of more complex and smooth profile using the proposed strategy. Microfluidic molds were designed using the commercial software 3Ds Max and fabricated using a high-resolution 3D printer (Makerbot Replicator 2X). The PDMS was fabricated by casting the printed molds. A delta-shuttle shaped microchannel was fabricated using the 3D printing based method. The results are shown in Fig. S2,† indicating a smooth linear profile with high precision. In conclusion, soft lithography is a well-established fabrication technique with high resolution. The paper-based fabrication approach provides a rapid and simple means to assemble multilayer structures. The 3D printing based method allows the fabrication of channel molds with a smooth profile, but it requires a high-resolution 3D printer. These fabrication methods are complementary to one another, which might be suitable for different occasions.

Assembly of linear gradients in cell density

To validate the proposed strategy, we initially attempted the assembly of linear gradients in cell density. Three stair-shaped microchannels were fabricated using soft lithography and rapid prototyping method (Fig. S1†). Each stair had 8 steps with identical width and rise (the vertical distance between the two adjacent steps). The step rises of the three stairs were set to 30, 60 and 90 μm, respectively, to yield three different slopes. Through diaphragm holes were punched at each end of the microchannels as the world-to-chip interface. After the PDMS microchannels were reversibly bonded to a fibronectin-coated glass substrate to form the final devices, homogeneous NIH 3T3 cell suspensions with a concentration of 6.0×10^5 cells mL^{-1} were loaded into the microchannels by pressure difference. The microfluidic devices were then incubated at 37 °C under a 5% CO_2 atmosphere. After sedimentation for 10 min, cells settled on the glass substrate by gravity to form cell gradients. The microfluidic devices were further incubated for ~2 h, allowing the cells to adhere to the substrate. Subsequently, cells were fluorescently labeled with Fluo-3, and the results are shown in Fig. 2b. As expected, the cell density increased along the stairs in all three microchannels. In addition, the higher the step rise, the greater the increasing rate was observed for the cell density. As shown in Fig. 2c, the cell densities in the three microchannels could be well fitted with linear functions. The correlation coefficients of the linear regressions (R^2) were 0.992, 0.995 and 0.997 for the microchannels with step rises of 30, 60, and 90 μm, respectively. The slopes of the regression lines were calculated to be 17.9, 35.7 and 52.9 cells mm^{-2}, respectively, which were consistent with the theoretical calculations (18, 36 and 54 cells mm^{-2}). These results validated that the fabricated microfluidic devices were able to establish linear gradients in cell density with high precision. Cell gradient profile was also dependent on the original cell density in the solution. Linear profiles were generally observed for cell suspensions of various concentrations (Fig. S3†). The higher the concentration, the larger the slope was found for a wide range of original cell density. We further tested cell viability on the microfluidic device. Results showed that over 90% cells remained alive in the microchannel after incubation for 10 h at 37 °C under a 5% CO_2 atmosphere, indicating good biocompatibility of both glass and PDMS as previously reported.

The established cell gradients were ladder like in the microscale. However, from the point of the entire microchannel, the cell gradients are in linear distribution. To achieve a smoother linear profile, 3D printing was used to fabricate the channel molds with a linear profile. As shown in Fig. S4,† the densities of cells located in random positions of the microchannel could be well fitted with a linear function. The correlation coefficient of the linear regressions (R^2) was 0.997.

Assembly of cell gradients with pre-defined profiles

Under *in vivo* tissue environment, the gradients in cell density are more complex than that of the single linear profile. Thus, arbitrary control over the cell gradient profile is sometimes necessary for reconstructing functional tissues, especially the interface tissues. Next, we fabricated two stair-shaped PDMS microchannels using a paper-based prototyping method (ESI†), which allowed control over the height of each layer, *i.e.*, the step rise, enabling us to generate cell gradients of exponential ($y = 30 \times 2x^{-1}$; unit, cells mm^{-2}) and piecewise
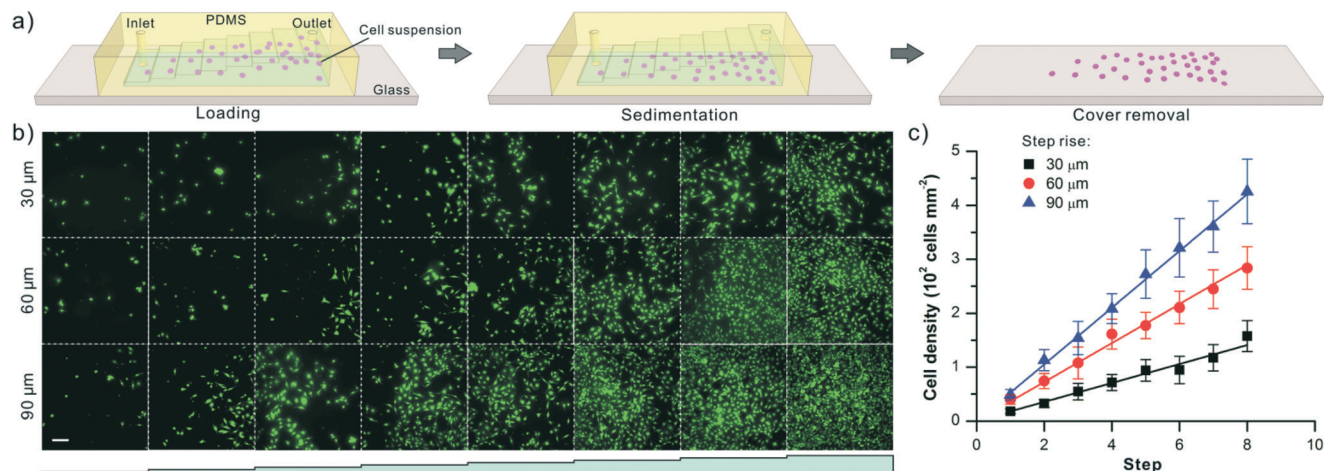
Fig. 2 Assembly of linear gradients in cell density. a) A cartoon illustrating the process for establishing cell gradients on a glass substrate using a stair-shaped microfluidic channel. b) Fluorescence images of Fluo-3 labeled NIH 3T3 cells at each step of the microchannels with the step rise of 30, 60 and 90 μm, respectively. The schematic at the bottom of the panel indicates the approximate locations in the microchannels for image acquisition. Scale bar, 50 μm. c) A graph summarizing the cell densities at each step of the three microchannels fitted with linear functions.

linear ($y = 15 + 15x$, $x \leq 3$; $y = 30x - 30$, $x > 3$; unit, cells mm^{-2}) profiles. After homogeneous NIH 3T3 cell suspensions with concentrations of 3.0×10^5 and 1.5×10^5 cells mL^{-1} were loaded into the microchannels with the exponential and the piecewise linear profiles, respectively, the microfluidic devices were incubated at 37 °C under a 5% CO_2 atmosphere for sedimentation of cells and generation of cell gradients. Fig. 3a and b show the distributions of cells at each step of the two microchannels after Fluo-3 labeling. Quantitative analyses are summarized in Fig. 3c and d. Results indicated that the cell densities in the two microchannels could be well fitted with exponential ($y = 27.0 \times 2x^{-1}$; unit, cells mm^{-2}) and piecewise linear ($y = 13.1 + 13.1x$, $x \leq 3$; $y = 27.5x - 30.4$, $x > 3$; unit, cells mm^{-2}) functions ($R^2 > 0.99$), which were in good agreement with the initial designs of the microchannels. The above results demonstrated that cell gradients of pre-defined profiles could be achieved using the developed method by controlling the height of each layer during the fabrication of the 3D microchannels.

Assembly of two overlapping cell gradients

In functional tissues, such as the interface tissue, there are often overlapping cell gradients of two or more cell types.[31] For example, in the tendon-to-bone insertion, the density of osteoblasts increases from tendon to bone and the density of fibroblasts changes in the opposite direction. Thus, we further explored the use of the developed method to assemble two oppositely overlapping cell gradients of different cell types on the same glass substrate. Before the experiments, NIH 3T3 and HepG2 cells were fluorescently labeled with DiI (red) and DiO (green), respectively. A stair-shaped PDMS microchannel with a linear profile (step rise, 90 μm) was reversibly bonded to a glass substrate. NIH 3T3 cells with a concentration of 6.0×10^5 cells mL^{-1} were loaded into the microchannel and incubated at 37 °C under a 5% CO_2

atmosphere for ~2 h, allowing adhesion of cells to the substrate. The glass substrate was then separated from the PDMS microchannel and briefly rinsed with culture media to remove unattached NIH 3T3 cells. Following a 180-degree rotation horizontally, the PDMS microchannel was reversibly bonded back to the same substrate. HepG2 cells with a concentration of 5.5×10^5 cells mL^{-1} were then loaded into the microchannel. After incubation at 37 °C under a 5% CO_2 atmosphere for two more hours, two oppositely overlapping cell gradients of different cell types were established. As shown in Fig. 4a, the densities of NIH 3T3 and HepG2 cells increased along the stairs as indicated by the schematic in the top and bottom panels. Calculations showed that the distributions of both cells could be well fitted with linear functions (Fig. 4b). The correlation coefficients of the linear
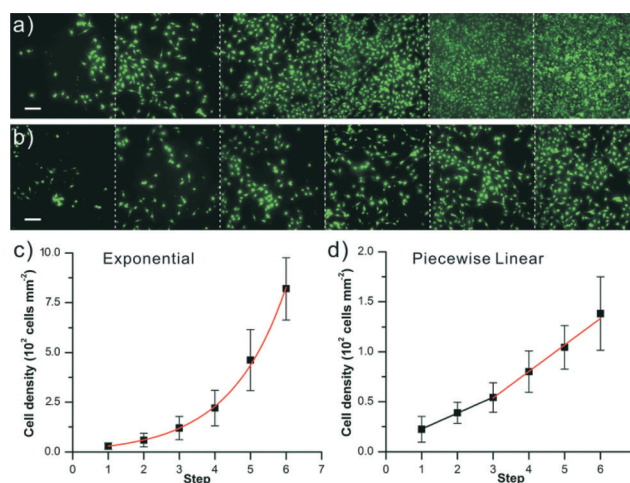

Fig. 3 Assembly of cell gradients with pre-defined profiles. Fluorescence images of Fluo-3 labeled NIH 3T3 cells at each step of the stair-shaped microchannel with an exponential (a) and a piecewise linear (b) profile. Data were summarized in (c) and (d) with exponential and piecewise linear fittings, respectively. Scale bar, 50 μm.

regressions were 0.994 and 0.998 for NIH 3T3 and HepG2 cells, respectively. The absolute values of the slopes were 53.9 and 48.4 cells mm^{-2}, which were in close agreement with the theoretical calculations of 54 and 49.5 cells mm^{-2}.

Assembly of two overlapping cell gradients with pre-defined designs

The above experiments demonstrated the capability of the 3D microfluidic strategy for assembling overlapping cell gradients of different cell types. In reality, cell gradients can not only overlap with one another but also exist in complex geometry. To push our method farther, we fabricated two 3D PDMS microchannels using the paper-based prototyping method (ESI†). The designs of the two microchannels are shown in the top (microchannel 1) and middle (microchannel 2) panels of Fig. 5a. In the radial direction, both microchannels were of a linear profile with a step rise of 100 μm. The expected distribution of cells is given in the bottom panel of Fig. 5a. To generate cell gradients, microchannel 1 was firstly bonded to a glass substrate. Homogeneous suspension of DiO-labeled HepG2 cells with a concentration of 9.0×10^5 cells mL^{-1} was loaded into the microchannel to establish the first cell gradient. Following removal of microchannel 1, the glass substrate was briefly rinsed with culture media and reversibly bonded to microchannel 2. Homogeneous suspension of DiI-labeled NIH 3T3 cells with a concentration of 9.0×10^5 cells mL^{-1} was then loaded into the microchannel to establish a second cell gradient on top of the first one. Fig. 5b–e show overlays of the fluorescence images of NIH 3T3 and HepG2 cells acquired at the locations indicated in the bottom panel of Fig. 5a. The results are summarized in the histogram of Fig. 5f. The distributions of both cells could be well fitted with linear functions in the radial direction with correlation coefficients of 0.999. The absolute values of the slopes were 91.8 and 94.6 cells mm^{-2} for NIH 3T3 and HepG2 cells, respectively, which were relatively consistent with the theoretical calculations of 90 cells mm^{-2}.
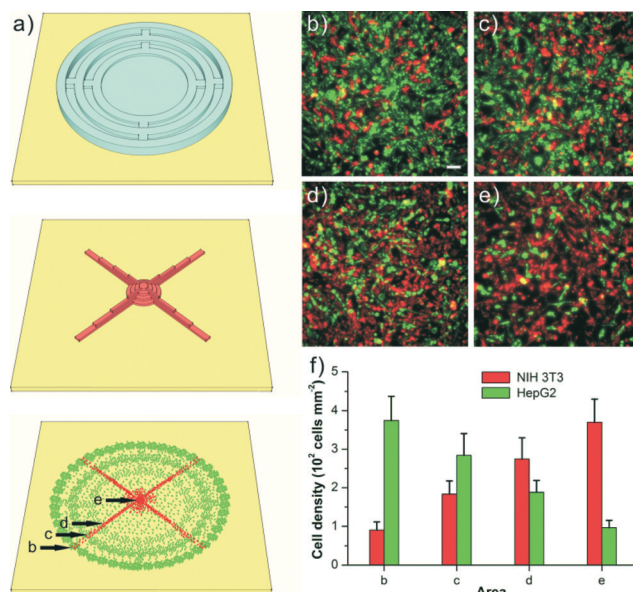

Fig. 5 Assembly of two overlapping cell gradients with pre-defined designs. a) Schematics illustrate the 3D microchannel designs for establishing cell gradients of HepG2 (top panel) and NIH 3T3 (middle panel) cells on the same glass substrate. The bottom panel illustrates the expected distributions of HepG2 (green) and NIH 3T3 (red) cells. b–e) Overlays of the fluorescence images of HepG2 (red) and NIH 3T3 (green) cells acquired at the locations indicated in the bottom panel of a). Scale bar, 50 μm. f) A histogram summarizing the cell densities in b–e.

Gradient in cell density regulates cell viability and proliferation

Controllable gradient in cell density helps in understanding how the change in cell density affects the behaviors of cells through the establishment of ECM cues or the regulation of cell–cell interactions. Additional experiments were carried out to show how the change in cell density regulates and affects the cell behaviors including cell viability, proliferation, and response to nano-CdTe quantum dots (QDs). Live/Dead assay was firstly carried out to validate the cell viability in the assembled cell gradient. Live cells were stained with Calcein-
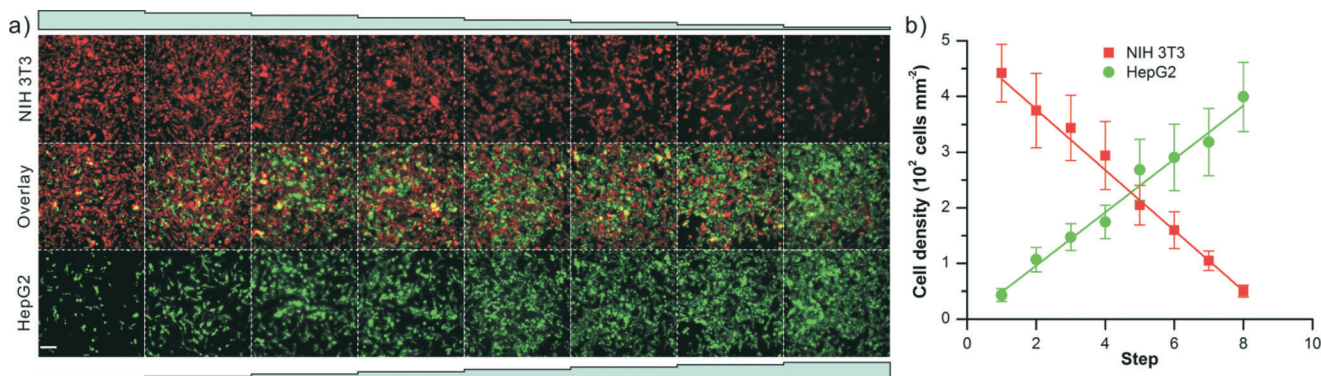

Fig. 4 Assembly of two overlapping cell gradients. a) Fluorescence images of DiI-labeled NIH 3T3 cells (red) and DiO-labeled HepG2 cells (green) on the same glass substrate after the establishment of the two cell gradients. The schematics at the top and bottom of the panel indicate the approximate locations for acquiring the images of NIH 3T3 and HepG2 cells, respectively. Scale bar, 50 μm. b) A graph summarizing the cell densities at each step of the microchannel fitted with linear functions.
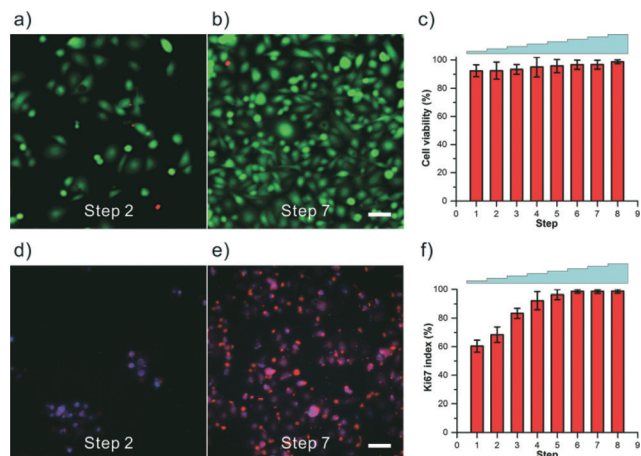
Fig. 6 Cell behavior was regulated by the cell gradient. a and b) A fluorescence image of cells stained with Calcein-AM and PI in cell viability assay. Scale bar, 30 μm. c) Summary of the cell viability measured in each step of a stair-shaped microchannel with a linear profile (step rise, 90 μm). d and e) Fluorescence images of cells stained with anti-Ki67 and DAPI in cell proliferation assay. Scale bar, 50 μm. f) Summary of the cell proliferation rate measured in each step of a stair-shaped microchannel with a linear profile (step rise, 90 μm).

AM, while dead cells were stained with propidium iodide. Results showed that the cell viability increased with increasing cell densities (Fig. 6a–c). Ki67 is a specific nuclear proliferation marker, which was used to study the proliferation capacity of cells with various densities. Cells stained with Ki67 were actively proliferating. Results indicated that cells were more actively proliferating in areas of high cell density than of low cell density (Fig. 6d–f). The cell behaves differently in cell gradients, which was regulated by the changes in cell density through the establishment of ECM cues or the regulation of cell–cell interactions. Experiments on cell gradient provided us better understanding of complex biological processes.

Nano-QD cytotoxicity assay with cell gradient in density

A cytotoxicity experiment of nano-CdTe QDs was carried out to study the response of cells with various densities (Fig. 7a).
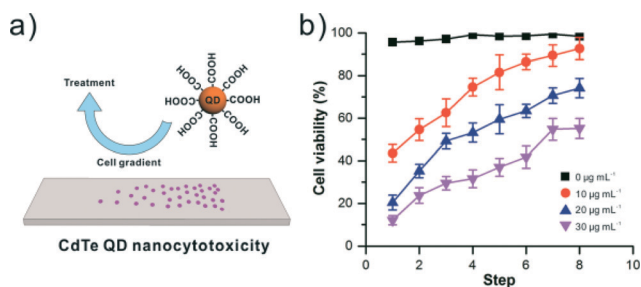

Fig. 7 a) Schematic of the CdTe QD cytotoxicity assay. b) CdTe QDs coated by carboxyl groups at concentrations of 0, 10, 20, and 30 μg mL^{-1} were used for cytotoxicity assay of cell gradients. Cell viability was validated in each step of a stair-shaped microchannel with a linear profile (step rise, 90 μm).

CdTe QDs coated by carboxyl groups were used in this cytotoxicity study. A stock solution of CdTe QDs was diluted in cell culture medium with the final concentrations of 0, 10, 20, and 30 μg mL^{-1} prior to use. After 24 h culturing, Live/Dead cell assay was carried out to validate how cell gradients responded to the cytotoxicity of the nanomaterial. Results showed that the cytotoxicity of QDs was dependent on the cell density at a given concentration of QDs. Cells with a higher density were more resistant to the cytotoxicity of CdTe QDs (Fig. 7b).

Conclusions

Our results strongly suggested that the proposed method could be used to assemble multiple overlapping cell gradients of pre-defined designs. In fact, there are several advantages associated with the 3D microfluidic strategy in comparison to previously reported methods. First, the developed method was rapid and robust. Generally, cell gradients could be established in 10 min due to the size of the microchannel in the microscale range. Full attachment of cells could be achieved after two-hour incubation at 37 °C under a 5% CO$_2$ atmosphere with a recovery of more than 90%. Second, this method did not use mechanical, electrical or chemical cues to establish cell gradients, thus maintaining the functionality of the target cells, which was critical for studies involving stem-cell differentiation or primary-cell types that must maintain their phenotypes. Another advantage of this method was its high controllability over the cell gradients. By simply controlling the height of each layer during the fabrication of the 3D microchannels, it could adequately generate cell gradients of pre-defined profiles, such as exponential and piecewise linear profiles, which were difficult to achieve using previously reported methods. As discussed in the results section, the reconstituted cell gradient profiles were always consistent with the pre-defined profiles. Furthermore, the established fabrication methods for PDMS microchannels allowed the production of microchannels of pre-defined designs, enabling the assembly of multiple overlapping cell gradients of different cell types by sequential cell seeding.

In conclusion, we demonstrated a versatile 3D microfluidic strategy for assembly of multiple cell gradients. Our results demonstrated that cell behaviors were regulated by the changes in cell density. QD cytotoxicity assay was also carried out to show the cell density-dependent results. It provided a simple and robust solution to precisely control the distribution of cells on the substrate, opening up a new avenue for reconstructing functional tissues.

Acknowledgements

Notes and references

1 E. S. Place, N. D. Evans and M. M. Stevens, *Nat. Mater.*, 2009, **8**, 457–470.

2 H. H. Lu, S. D. Subramony, M. K. Boushell and X. Z. Zhang, *Ann. Biomed. Eng.*, 2010, **38**, 2142–2154.

3 S. MacNeil, *Nature*, 2007, **445**, 874–880.

4 K. L. Moffat, I. N. E. Wang, S. A. Rodeo and H. H. Lu, *Clin Sports Med.*, 2009, **28**, 157.

5 A. Seidi, M. Ramalingam, I. Elloumi-Hannachi, S. Ostrovidov and A. Khademhosseini, *Acta Biomater.*, 2011, **7**, 1441–1451.

6 S. N. Bhatia, U. J. Balis, M. L. Yarmush and M. Toner, *FASEB J.*, 1999, **13**, 1883–1900.

7 F. Rosso, A. Giordano, M. Barbarisi and A. Barbarisi, *J. Cell. Physiol.*, 2004, **199**, 174–180.

8 M. Radisic, J. Malda, E. Epping, W. L. Geng, R. Langer and G. Vunjak-Novakovic, *Biotechnol. Bioeng.*, 2006, **93**, 332–343.

9 J. Chen, Y. Li, T. S. Yu, R. M. McKay, D. K. Burns, S. G. Kernie and L. F. Parada, *Nature*, 2012, **488**, 522.

10 L. C. You, R. S. Cox, R. Weiss and F. H. Arnold, *Nature*, 2004, **428**, 868–871.

11 S. Y. Cheng, S. Heilman, M. Wasserman, S. Archer, M. L. Shuler and M. M. Wu, *Lab Chip*, 2007, 7, 763–769.

12 C. L. E. Helm, M. E. Fleury, A. H. Zisch, F. Boschetti and M. A. Swartz, *Proc. Natl. Acad. Sci. U. S. A.*, 2005, **102**, 15779–15784.

13 D. H. Kim, C. H. Seo, K. Han, K. W. Kwon, A. Levchenko and K. Y. Suh, *Adv. Funct. Mater.*, 2009, **19**, 1579–1586.

14 L. Y. Liu, B. D. Ratner, E. H. Sage and S. Y. Jiang, *Langmuir*, 2007, **23**, 11168–11173.

15 A. M. D. Wan, D. J. Brooks, A. Gumus, C. Fischbach and G. G. Malliaras, *Chem. Commun.*, 2009, 5278–5280.

16 D. A. Lauffenburger and A. F. Horwitz, *Cell*, 1996, **84**, 359–369.

17 W. Y. Liu, Y. Zhang, S. Thomopoulos and Y. N. Xia, *Angew. Chem., Int. Ed.*, 2013, **52**, 429–432.

18 G. Yang, Y. Cao, J. Fan, H. Liu, F. Zhang, P. Zhang, C. Huang, L. Jiang and S. Wang, *Angew. Chem., Int. Ed.*, 2014, **53**, 2915–2918.

19 U. A. Gurkan, S. Tasoglu, D. Kavaz, M. C. Demirel and U. Demirci, *Adv. Healthcare Mater.*, 2012, **1**, 149–158.

20 A. Hasan, A. Paul, N. E. Vrana, X. Zhao, A. Memic, Y. Hwang, M. R. Dokmeci and A. Khademhosseini, *Biomaterials*, 2014, **35**, 7308–7325.

21 J. El-Ali, P. K. Sorger and K. F. Jensen, *Nature*, 2006, **442**, 403–411.

22 S. N. Bhatia and D. E. Ingber, *Nat. Biotechnol.*, 2014, **32**, 760–772.

23 A. Agarwal, J. A. Goss, A. Cho, M. L. McCain and K. K. Parker, *Lab Chip*, 2013, **13**, 3599–3608.

24 D. Huh, B. D. Matthews, A. Mammoto, M. Montoya-Zavala, H. Y. Hsin and D. E. Ingber, *Science*, 2010, **328**, 1662–1668.

25 Y. Torisawa, S. S. Catherine, T. Mammoto, A. Mammoto, J. C. Weaver, T. Tat, J. J. Collins and D. E. Ingber, *et al.*, *Nat. Methods*, 2014, **11**, 663–669.

26 P. J. Lee, P. J. Hung and L. P. Lee, *Biotechnol. Bioeng.*, 2007, **97**, 1340–1346.

27 B. J. Kane, M. J. Zinner, M. L. Yarmush and M. Toner, *Anal. Chem.*, 2006, **78**, 4291–4298.

28 J. Wu, Q. Chen, W. Liu and J. M. Lin, *Lab Chip*, 2013, **13**, 1948–1954.

29 J. Wu, H. Li, Q. Chen, X. Lin, W. Liu and J. M. Lin, *RSC Adv.*, 2014, **4**, 24929–24934.

30 R. Ning, S. Wang, J. Wu, F. Wang and J. M. Lin, *Small*, 2014, **10**, 4113–4117.

31 S. J. Hollister, *Nat. Mater.*, 2005, **4**, 518–524.